LAWRENCE
LIVERMORE
NATIONAL
LABORATORY

LLNL-JRNL-411279

Moment enhancement in dilute magnetic semiconductors: MnxSi1-x with x = 0.1%

M. Shaughnessy, C. Y. Fong, R. Snow, K. Liu, J. E. Pask, L. H. Yang

March 16, 2009

Applied Physics Letters

Disclaimer

Moment enhancement in dilute magnetic semiconductors: Mn_xSi_{1-x} with $x = 0.1\%$

M. Shaughnessy,[1] C.Y. Fong,[1] Ryan Snow,[1] Kai Liu,[1] J.E. Pask,[2] and L.H. Yang[2]

[1]*Department of Physics, University of California, Davis, CA 95616-8677*

[2]*Condensed Matter and Materials Division, Lawrence Livermore National Laboratory, Livermore, CA 94551*

(Dated: March 13, 2009)

The experimentally determined magnetic moments/Mn, M, in Mn_xSi_{1-x} are considered, with particular attention to the case with 5.0 μ_B/Mn, obtained for $x = 0.1\%$. The existing theoretical M values for neutral Mn range from 2.83 to 3.78 μ_B/Mn. To understand the observed $M = 5.0\mu_B$/Mn, we investigated Mn_xSi_{1-x} for a series of Mn concentrations and defect configurations using a first-principles density functional method. We find a structure in which the moment is enhanced. It has $5.0\mu_B$/Mn, the Mn at a substitutional site, and a Si at a second-neighbor interstitial site in a large unit cell. Subsequent analysis shows that the observed large moment can be understood as a consequence of the weakened d-p hybridization resulting from the introduction of the second-neighbor interstitial Si and substantial isolation of the Mn–second-neighbor Si complex at such concentrations.

Key Words: Dilute magnetic semiconductors, enhanced magnetic moment, substitutional and interstitial sites

PACS numbers: 75.50.Pp, 71.20.Be

Spintronic devices, which exploit the electron spin as well as its charge, hold the promise of breakthroughs for sensors, memory chips, microprocessors, and a host of other applications [1, 2]. Among the candidate materials for spintronic devices, dilutely doped transition elements in III-V compounds have been among the most studied. However, issues of sample quality [3] and low Curie temperature [2] have limited their usefulness for spintronic applications in practice. Recently, dilute alloys of Mn_xSi_{1-x} have attracted attention after reports [4, 5] of epitaxially grown thin films of Mn_xSi_{1-x} with $x = 5.0\%$ that exhibit the anomalous Hall effect at ∼70 K. The demonstration of magnetic properties in Si-based materials and the greater maturity of Si-based technologies relative to those of other semiconductors enhance the prospects for utilizing Mn_xSi_{1-x} to realize spintronic devices. Among more recent experiments on Si-based alloys [6–8], Refs. [7] and [8] report the magnetic moment/Mn, M (Table I). At $x = 0.1\%$, an M of 5.0 μ_B/Mn is found. This value is the maximum achievable when all five d-electron spins align and therefore is particularly interesting that it occurs in the solid alloy. A number of calculations [9–13] have been carried out with Mn in a variety of configurations in various supercells. The total number of atoms in the supercells range from 32 to 218. Only when imposing a 2+ charge state on the Mn has the observed $M = 5.0\mu_B$/Mn been reproduced [11]. We summarize the M values found in recent works in Table I, where the Mn sites are tetrahedral interstitial (TI), hexagonal interstitial (HI), and substitutional (S). In this Letter, we show for the first time that the large, experimentally observed 5.0 μ_B/Mn moment in Mn_xSi_{1-x} can in fact be achieved, without charge-state or other such constraints, in the presence of interstitial defects at sufficiently low Mn concentrations. The mechanism found is quite general and so may be operative in other such dilute magnetic semiconducting or half-metallic systems.

TABLE I: Summary of M values. For experiments, doping level x is specified. For theory, model and charge states are given.

Experiment Doping Level, x	$M(\mu_B$/Mn)	Reference		
0.1%	5.0	[7]		
0.8%	1.5	[7]		
1.0%	4.15	[8]		
1.5%	4.05	[8]		
Theory				
Model	**Site**	**Charge State**	M	**Reference**
64-atom-surface			3.14	[9]
218-atom-surface	bridge		3.78	[10]
2x1 reconstruction	(top layer)		3.78	[10]
Below surface	I (3rd layer)		3.0	[10]
	I (4th layer)		2.95	[10]
216-atom	TI	Mn^{2+}	5.0	[11]
		Mn^0	3.0	[11]
2 Mn in 128-atom	S		2.83	[12]
32-atom	HI		3.0	[13]
	TI		3.0	[13]
	S		3.0	[13]

During the ion implantation [7] and arc melting [8] growth of dilute Si-based alloys, no particular charge state of the Mn is prepared. Therefore, we consider the following questions: Is the Mn^{2+} charge state necessary to obtain the maximum M in Si based alloys? If not, what possible configuration of Mn and Si can give $M = 5.0\mu_B$/Mn? To answer these questions, we carried out an extensive series of *ab initio* density functional calculations on a range of periodic models. A planewave

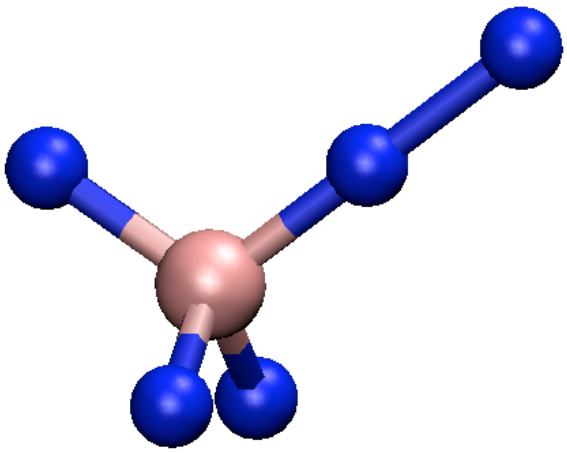

FIG. 1: The Mn and its neighboring Si atoms. The Mn atom is the large (lighter) central sphere and the Si atoms are smaller (darker) spheres. The sn Si of the Mn is shown in the upper right at the TI site, and the "nn Si" is shown between it and the Mn. The other atoms in the 513-atom cell are omitted for clarity.

basis and ultrasoft pseudopotentials [15] were employed, with Perdew91 GGA exchange-correlation [16], 650 eV planewave cutoff, and (3,3,3) Monkhorst-Pack k-point mesh. The alloy was modelled by a single Mn atom in supercell models containing 64, 216, and 512 Si atoms with different configurations for the Mn including S, TI, and HI. Among all models, only one was found to have the observed 5.0 μ_B/Mn. This configuration has (1) a Mn in its neutral charge state at an S site, (2) a Si occupying a TI site serving as a second neighbor (sn) to the Mn, and (3) a large, 513 atom unit cell.

The 513-atom cell consists of a $4 \times 4 \times 4$ supercell of conventional 8-atom diamond cells, with substitutional Mn and sn interstitial Si. The bond length is 2.36Å corresponding to a 5.46Å lattice constant as compared to the experimental value of 5.43Å. The lattice constant is optimized on the 2-atom Si primitive cell of the diamond structure. In Fig. 1, we show the portion of the supercell containing the Mn, its nearest neighbor (nn) Si's, and second-neighbor (sn) Si interstitial after all atoms are relaxed to forces less than 6.0 meV/Å. Hereafter, we refer to the nn Si between the Mn and sn Si as *the* nn Si due to its unique role in the present context.

We emphasize that only the model with the Mn at the S site, sn Si at the TI site, and 513 atom unit cell gives the 5.0 μ_B moment. The impurity atom and its sn Si need to be well isolated from neighboring periodic images. The corresponding concentration of doping in this model is 0.19%, about a factor of 2 larger than the concentration in the experiments [7]. Before relaxation, the maximum component of the force at the most distant Si from the Mn is already small at 0.015 eV/Å. In the corresponding 217-atom cell, the corresponding components are 0.08 eV/Å. Therefore, the Mn—nn-Si—sn-Si complex is well isolated in the 513-atom model. The need for this degree of isolation will be clarified below.

Without the sn Si, the nn Si displaces away from the Mn atom by 0.04 Å compared to the unrelaxed case. This is consistent with Ref. [8], which suggests the Mn atoms are at the S sites because of an observed expansion of the Si lattice constant. With the sn Si, the relaxation happens in the vicinity of the Mn—nn-Si—sn-Si complex. Because the four neighbors of the sn Si already have four bonds, the sn Si doesn't form covalent bonds. Upon relaxation, the Mn and nn Si displace away from the sn Si but the sn Si follows such that the bond length remains at the equilibrium value of 2.36 Å (experimentally, 2.35 Å). Because the relaxed sn-Si–nn-Si separation is smaller than the distances to its other three neighbors, the sn Si at the TI site shifts some of its charge toward the nn Si, as we discuss below. While both models show a local expansion around the Mn, the distance between the Mn and its other three nn Si atoms is 2.38 Å in the sn model, 0.02 Å less than in the model without the sn Si (nsn model).

According to the ionic model [18], a Mn atom at an S site in Si should have a magnetic moment of 3.0 μ_B/Mn owing to four of its seven electrons hybridizing with the four neighboring Si atoms. The three remaining electrons at the Mn align their spins in accordance with Hund's rule to give the stated magnetic moment. In the 512-atom cell with no sn Si, the calculated moment is in fact exactly 3.0 μ_B/Mn. Any greater moment in experiment or theory indicates some enhancement.

The bonding between the nn Si and its three Si neighbors is of sp^3 type while that between the nn Si and Mn shows strong d-p hybridization. Figure 2(a) shows the charge density of the majority (down) spin channel in the vicinity of the Mn and nn Si in the nsn model. The minority (up) spin charge density (not shown) is qualitatively similar. The dense (brightly colored online) contours in the bottom left of the figure correspond to the large d-electron density in the vicinity of the Mn. The d-p hybrid bonding between the Mn and nn Si differs from the bonding between the nn Si and its other neighbors, as manifested in the distinct charge distributions between the atoms. The covalent bonds between Si atoms exhibit the characteristic dumbbell shape, with the maxima near host atoms.

Figure 2(b) shows the charge density in the same spin channel as in 2(a) but for the sn model. In the presence of the sn Si, the sp^3 orbital of the nn Si that participated in the d-p bonding is *pulled away* from the Mn, thus reducing the hybridization. The charge distribution between the nn Si and sn Si shows an asymmetric dumbbell shape indicating that the nn Si shifts some of its charge toward the sn Si and away from the Mn. When the bond between the Mn and nn Si is weakened in the

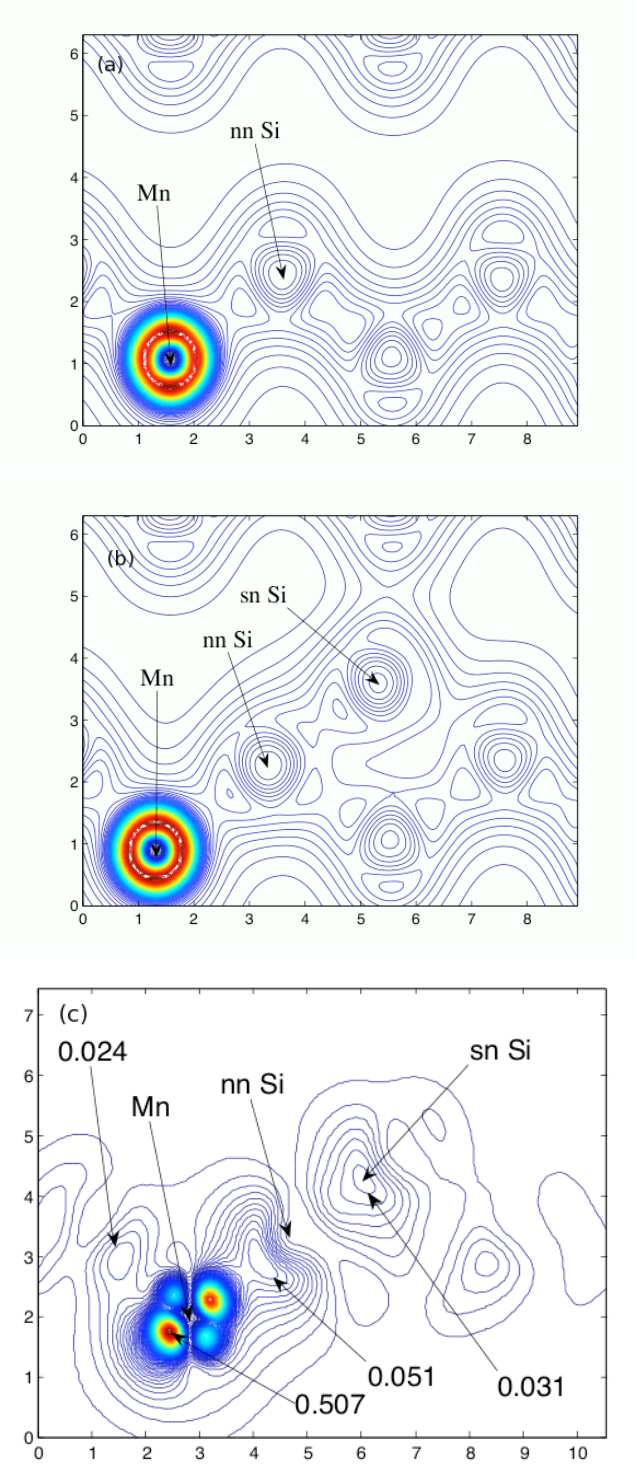

FIG. 2: The total charge density in the majority (down) spin channel for (a) the nsn model and (b) the sn model. The bottom panel (c) shows the spin density difference as given in Eq (2), with the centers of the Mn aligned. The labels show the positions of the relevant atoms and selected contour values ($e/\text{Å}^3$). All distances are in Å. The **x**-axis of the partial cross-section is the [110] direction of the supercell and the **y**-axis coincides with the **z**-axis of the supercell

presence of the sn Si, the two electrons in the bond retreat toward their respective host atoms. The maximum charge densities along the bond between the Mn and nn Si in front of and behind the Mn atom, increase by ∼13% and ∼9%, respectively, relative to the case without the sn Si. Along the same line, the maximum nearer to the nn Si increases by ∼5% and moves closer to the nn Si by ∼7%, relative to the case without the sn Si. From an atomic point of view, the addition of the sn Si reduces the hybridization between the Mn d-orbital and the nn Si sp^3 states. The electron retreating to the Mn aligns its spin in accordance with Hund's rule and the ferromagnetic exchange polarizes the density around the nn Si. As we show below, the polarization is not well localized.

To quantify the weakening of the d-p hybridization, we computed the density of d-states (d-DOS) in the down spin channel with and without the sn Si and computed the variances of the distributions. The variance of d-DOS for the sn model was found to be 4.08 eV^2 while that for the nsn model was 4.53 eV^2 in an energy window from E_f to 3.0 eV below. The narrower width of the d-DOS in the presence of the sn Si confirms the weakening of the d-p hybridization suggested by the corresponding charge distribution.

The difference of total spin up and spin down charge is $3e$ and $5e$ in the nsn and sn cases, respectively. As a consequence of the weakened d-p hybridization, the local moment around the Mn is about 4 μ_B. The residual weak spin polarization in the rest of the unit cell contributes approximately 1 μ_B to the total moment and consequently, the M value for the relaxed dilute Mn_xSi_{1-x} is 5.0 μ_B/Mn in agreement with the measured value after the sample is annealed [7].

Figure 2(c) illustrates the effect of the sn Si on the magnetic moment distribution by showing the difference $\Delta\sigma(\mathbf{r})$ of the spin densities with and without the sn Si. The spin density is defined as

$$\sigma(\mathbf{r}) = \rho(\mathbf{r})_{down} - \rho(\mathbf{r})_{up} \quad (1)$$

The contours are determined by the difference of spin densities

$$\Delta\sigma(\mathbf{r}) = \sigma(\mathbf{r})_{sn} - \sigma(\mathbf{r})_{nsn}, \quad (2)$$

where first and second terms on the right hand side are related to the densities with and without the sn Si, respectively. The spin densities derived from Figs. 2(a) and 2(b) are not directly subtracted because the atomic positions differ upon relaxation. Instead, both densities are determined with the sn model atomic positions.

In Fig. 2(c), the distribution near the Mn shows the four lobes of a d-state with some of its charge shifted from the lobe pointing to the nn Si back to the open region behind the fourfold-coordinated Mn atom. The dense region (brightly colored online) in the lower left, shows the strong positive $\Delta\sigma(\mathbf{r})$ due to the d-electron's retreat as

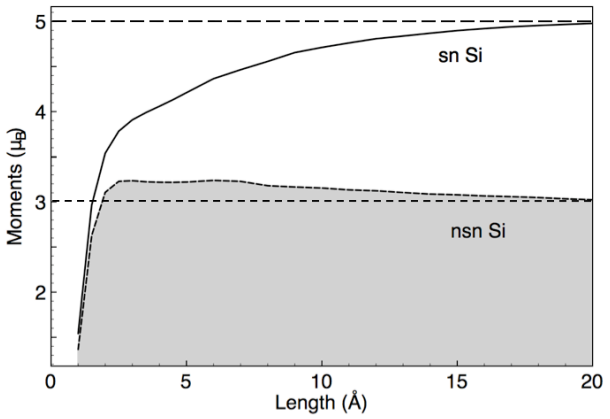

FIG. 3: Integrated moment within a Mn-centered cube as a function of cube side length.

the d-p hybridization is weakened. The (blue online) side contours near the nn Si indicate a sidewise displacement of the sp^3 orbital into the open space around the bond after it retreats to the nn Si. The overlap of the wavefunctions as the sn Si shifts some of its charge toward the nn Si induces some moment near the sn Si, indicated by the contours in Fig. 2(c) near the sn Si. The labeled values of the contours in Fig. 2(c) show the dominant effect is a large change in the immediate vicinity of the Mn atom with smaller changes in moment near the nn and sn Si. The reduced d-p hybridization allows for the sp^3 electron of the nn Si to spill out into the empty region surrounding the bond, reducing the spatial overlap of the d and sp^3 electrons and making their spin alignment more energetically favorable.

Figure 3 shows the total magnetic moment in the alloy as a function of distance from the Mn, with and without the sn Si. The results are obtained by integrating the spin densities of the two cases in a series of cubes of increasing size centered on the Mn. For the case with the sn Si, as the size of the integration volume increases to fill the cell, the moment reaches 5 μ_B/Mn while in the case without the sn Si, it reaches 3 μ_B/Mn. The monotonic increase of M with increasing volume around the Mn in the sn Si case suggests a reason for the smaller moments found at higher Mn concentrations previously: the operative exchange interactions are long ranged, substantial over several bond lengths, so that smaller concentrations are required for sufficient isolation to realize the full 5 μ_B/Mn moment. Details of the differing long range polarizations, and associated exchange mechanisms, in each case will be presented elsewhere [14].

In summary, we found that the experimentally observed 5.0 μ_B/Mn moment in Mn_xSi_{1-x} with $x = 0.1\%$ can only be accounted for, among all models considered, by an isolated Mn at an S site coupled with sn Si at a TI site in a sufficiently large unit cell. The concentration x of the unit cell considered corresponds to 0.19%, about a factor of two larger than experiment. Based on the mechanism proposed it is predicted that smaller concentrations, corresponding to more computationally demanding models, will yield precisely the same M. Our results for models with smaller unit cells, like those in previous works, do not produce this observed magnetic moment due to long range interactions with neighboring complexes. The picture which emerges for the 5.0 μ_B/Mn moment in Mn_xSi_{1-x} is one in which the sp^3 orbital of the nn Si participating in the bonding with the Mn is pulled away from the Mn, reducing the d-p hybridization and leaving the Mn in a higher-spin, more atomic-like state. The Mn, nn Si, sn Si, and longer range polarization of the surrounding lattice all contribute to the measured moment, with the Mn atom giving the dominant contribution. It will be of interest to consider this mechanism of moment enhancement in other dilute magnetic semiconducting and/or half metallic systems as well.

This work was supported by the NSF Grant No. ECCS-0725902. Work at Lawrence Livermore National Laboratory was performed under the auspices of the U.S. Department of Energy under Contract DE-AC52-07NA27344.

[1] Y. Ohno, D.K. Young, B. Beschoten, F. Matsukar, H. Ohno, and D. Awschalom, Nature **402**, 790 (1999).
[2] P. Ball, Nature **404**, 918 (2000).
[3] M.L. Reed et al., Appl. Phys. Lett. **79**, 790 (2001).
[4] H. Nakayama, H. Ohta, and E. Kulatov, Physica B **302-303**, 419 (2001).
[5] Y.D. Park et al. Science **295**, 651 (2002).
[6] F.M. Liu, X.C. Gao, X.S. Wu, Y.W. Du, H. Zhu, J.Q. Xiao, and P. Chen, Appl. Phys. Lett. **85**, 786 (2004).
[7] M. Bolduc, A. Stollenwerk, V.P. LaBella et al., Phys. Rev. B **71**, 033302 (2005).
[8] S.B. Ma, Y.P. Sun, B.C Zhao, P. Tong, X.B. Zhu, and W.H. Song, Solid State Comm. **140**, 192 (2006).
[9] G.M. Dalpian, A.J.R. da Silva, and A. Fazzio, Phys. Rev. B **68**, 11310 (2003).
[10] A.J.R. da Silva, A. Fazzio, and A. Antomelli, Phys. Rev. B **70**, 193205 (2004).
[11] F Bernardini, S. Picozzi, and A. Continenza, Appl. Phys. Lett. **84**, 2289 (2004).
[12] H. Weng and J. Dong, Phys. Rev. B **71**, 035201 (2005).
[13] Z.Z. Zhang, B. Partoens, K. Chang, and F.M. Peeters, Phys. Rev. **77**, 155201 (2008).
[14] M. Shaughnessy et al. In preparation (2009).
[15] VASP, Institute fur Theoretische Physik of the Technishe Universitat, Wien, Austria
[16] J.P. Perdew, K. Burke, and M. Ernzerhot, Phys. Rev. Lett. **77**, 3865 (1996).
[17] H.J. Monkhorst and J.D. Pack, Phys. Rev. B **13**, 5188 (1976).
[18] C.Y. Fong, M.C. Qian, K. Liu, L.H Yang, and J.E. Pask, J. of Nanosci. and Nanotechnol. **8**, 3652 (2008).